CrystEngComm

PAPER

Orientation dependence of electrical properties of large-sized sodium potassium niobate lead-free single crystals

Cite this: DOI: 10.1039/c3ce42464b

Hao Deng,[ab] Xiangyong Zhao,[a] Haiwu Zhang,[ab] Chao Chen,[ab] Xiaobing Li,[a] Di Lin,[a] Bo Ren,[a] Jie Jiao[a] and Haosu Luo[a]

Received 3rd December 2013,
Accepted 7th January 2014

DOI: 10.1039/c3ce42464b

www.rsc.org/crystengcomm

Lead-free $(K_{0.25}Na_{0.75})NbO_3$ (KNN25/75) single crystals with dimensions of Ø30 × 10 mm were successfully grown by a top seeded solution growth technique (TSSG). The X-ray diffraction pattern shows that the as-grown crystals possess an orthorhombic perovskite structure. The concentrations of K, Na, and Nb elements in the as-grown crystal were measured by X-ray fluorescence analysis. The dielectric, ferroelectric and piezoelectric properties of KNN25/75 crystals with different orientations, *i.e.*, pseudocubic (100) and (110) ($(100)_{pc}$ and $(110)_{pc}$), were investigated. A higher piezoelectric constant d_{33} ~ 145 pC N^{-1} and electromechanical coupling coefficient k_t ~ 69% were observed along the $(100)_{pc}$ orientation compared with d_{33} ~ 70 pC N^{-1} and k_t ~ 51% along $(110)_{pc}$. However, when a bipolar electric field was applied, a two times higher strain value can be achieved in crystals oriented along $(110)_{pc}$ than along $(100)_{pc}$. These orientation dependent physical properties can be explained in the framework of domain engineering and the switching effect.

Introduction

Lead-based ferroelectrics such as lead zirconium titanate (PZT) ceramics[1–3] have been used in numerous practical applications such as sensors, actuators, ultrasonic transducers, *etc.* Due to the toxic nature of PbO, however, considerable recent studies have been focused on lead-free piezoelectric materials from an environmental protection viewpoint. As a member of lead free materials, alkaline niobate $(K_xNa_{1-x})NbO_3$ (KNN)-based solid solutions have been attracting much attention as they are believed to provide a relatively high piezoelectric response, a high Curie temperature and a high acoustic velocity. Since the great breakthrough made by Saito *et al.*[4] in textured KNN-based ceramics,[5] preparation of KNN ceramics with better piezoelectric properties has been extensively studied.[6–9] Provided that texture engineering can lead to an improvement in piezoelectric properties, single crystals of KNN are also expected to have superior properties. In addition, free from the effect of the grain boundary in ceramics, single crystals are more appropriate for investigating the nature of materials.

To obtain large-sized single crystals with excellent properties, great endeavor has been devoted to various growth methods. Solid-state single crystal growth (SSCG) has been adopted to grow KNN,[10–12] but the resulting crystal proved to be porous and with poor quality. The KNN crystals grown by a flux method, using fluxes such as NaF, a KF–NaF mixture and $NaBO_2$,[13–17] display enhanced quality, yet the size of the crystals is relatively small. Relatively large-sized KNN crystals were obtained by Saravanan *et al.*[18] by adding boron trioxide (B_2O_3) into the mixture of KF and NaF fluxes; the dielectric and piezoelectric properties were enhanced this way. The Bridgeman method has also been employed by Chen *et al.*[19] to grow large-sized Li-doped KNN crystals with a piezoelectric coefficient of up to 405 pC N^{-1}; nevertheless, the relatively high leakage current leads to unsaturated polarization hysteresis loops. Using the TSSG method, Davis *et al.* acquired large-sized Li-doped KNN crystals with a large k_t (≤70%).[20] Zheng *et al.*[21] found that Ta helps the growth of KNN crystals and obtained large-sized (K,Na)(Nb,Ta)O_3 (12 × 12 × 11 mm^3) crystals. Moreover, they reported a complete set of elastic, dielectric and piezoelectric constants for the $[001]_c$ poled domain engineered crystal. However, a systematic study on the dielectric, piezoelectric and ferroelectric properties as a function of the crystallographic orientation of pure KNN crystals has not been reported in literature up to now.

In this study, a high-quality and large-sized $(K_{0.25}Na_{0.75})NbO_3$ (KNN25/75) single crystal has been achieved by a carefully controlled TSSG method. The dimensions of the as-grown KNN25/75 single crystal reached up to Ø30 × 10 mm. The obtained KNN crystals provided us a superb material for the

[a] Key Laboratory of Inorganic Functional Materials and Devices, Shanghai Institute of Ceramics, University of Chinese Academy of Sciences, 215 Chengbei Road, Jiading, Shanghai 201800, China. E-mail: hsluo@mail.sic.ac.cn
[b] University of Chinese Academy of Sciences, Beijing, 100049, China

dielectric, piezoelectric, ferroelectric and electromechanical coupling property characterization along different orientations.

Experimental

$(K_{0.25}Na_{0.75})NbO_3$ single crystals were grown by a carefully controlled TSSG technique. The raw materials of K_2CO_3 (99.99%), Na_2CO_3 (99.99%), and Nb_2O_5 (99.99%) were weighed according to the nominal ratio of $0.70KNbO_3/0.30NaNbO_3$ to obtain KNN25/75 single crystals based on the $KNbO_3$–$NaNbO_3$ phase diagram in ref. 22. Then the well mixed compounds were put into a platinum (Pt) crucible and calcined at 850 °C for 3 h in air to form the KNN70/30 polycrystalline precursor. Then the polycrystalline materials were ground and mixed with excess ~20 wt% Na_2CO_3 and K_2CO_3 as self-flux. When heated above 850 °C, both Na_2CO_3 and K_2CO_3 decomposed, so the real flux was Na_2O–K_2O. Single crystals were grown using a $[001]_{pc}$ direction seed in a Pt crucible, which was heated to ~1160 °C using a resistance furnace under an air atmosphere. The velocities of rotation and pulling of the rod with the seed crystal were, respectively, ~16 rpm and ~3.0 mm per day. At the end of the crystal growth, the crystals were separated from the flux–melt surface and then slowly cooled down to room temperature.

The lattice structure of the as-grown crystal was determined by X-ray diffraction which was carried out using a Huber-G670 X-ray diffractometer (Cu $K_{\alpha1}$, λ = 1.5406 Å). The diffractograms of the $(100)_{pc}$ and $(110)_{pc}$ oriented single crystals were obtained using a Bruker D8 Discover HRXRD system. The concentrations of K, Na, and Nb elements in the as-grown crystal were measured by X-ray fluorescence analysis (XRF). Based on the measured results, the effective segregation coefficients of K and Na were calculated.

For the electrical property measurements, the as-grown KNN single crystals were sliced into wafers with a thickness of ~0.48 mm, perpendicular to their pseudocubic $[100]_{pc}$ and $[110]_{pc}$ directions. Then, all of the samples were sputtered with gold electrodes. The temperature dependence of the dielectric properties of unpoled samples was analyzed in the temperature range of 30–500 °C using an Agilent 4294A precision impedance analyzer. For the piezoelectric measurements, the crystal samples were poled in silicon oil at 180 °C for 15 min with a dc electric field of 40 kV cm^{-1} and then cooled to room temperature with half of the poling electric field. The d_{33} was tested using a Berlincourt quasistatic meter at 55 Hz. The electric field dependence of the polarization (P–E curves) and strain curves was characterized using a ferroelectric test system (aixACCT TF analyzer 1000) at room temperature.

Results and discussion

Fig. 1(a) shows the photograph of the as-grown KNN25/75 single crystal pulled along the $[001]_{pc}$ direction, with dimensions of up to Ø30 × 10 mm. The as-grown crystal is semi-transparent with no inclusions and exhibits four clear symmetrical growth ridges, indicating the cubic growth habit. A polished $(100)_{pc}$ wafer shown in Fig. 1(b) is transparent with several domain walls visible in it.

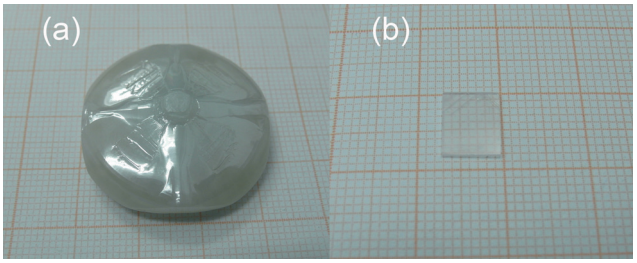

Fig. 1 (Color online) Photographs of (a) the as-grown KNN25/75 single crystal and (b) the polished KNN25/75 single crystal wafer.

The X-ray diffraction patterns of the KNN70/30 polycrystalline materials and powders of the as-grown single crystals are presented in Fig. 2(a). It is clear that both the raw materials and the KNN single crystals are of the perovskite-type structure. The splitting of the (200) cubic indexed peak at ~45°

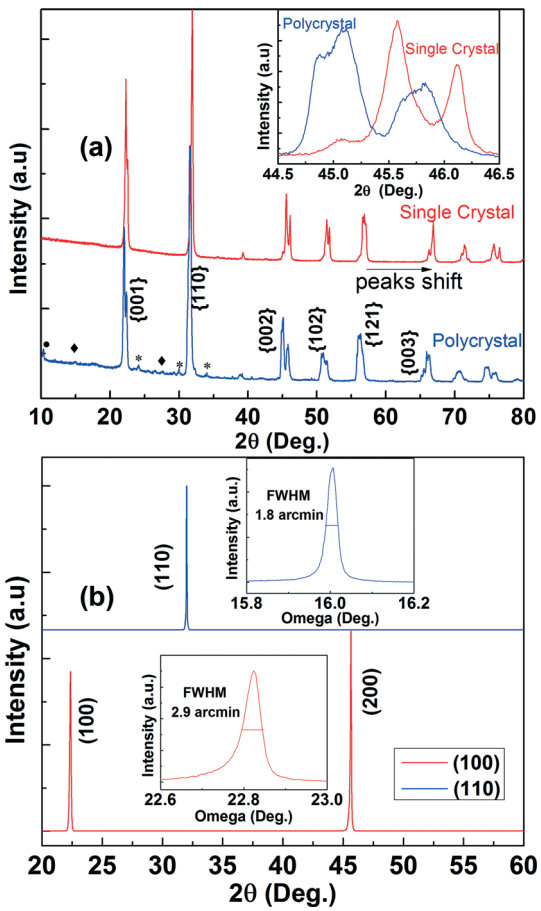

Fig. 2 (Color online) (a) XRD patterns of the KNN70/30 polycrystalline material and the powder of as-grown KNN25/75 single crystals. (Minor peaks may be attributed to: "•" – $K_4Nb_6O_{17}$ (PDF # 76-0977), "♦" – $K_3Nb_7O_{19}$ (PDF # 78-1395), and "*" – $KHCO_3$ (PDF # 12-0292).) (b) X-ray diffractograms of the (110)-oriented single crystal (top) and of the (100)-oriented single crystal (bottom). The insets show their respective rocking curves.

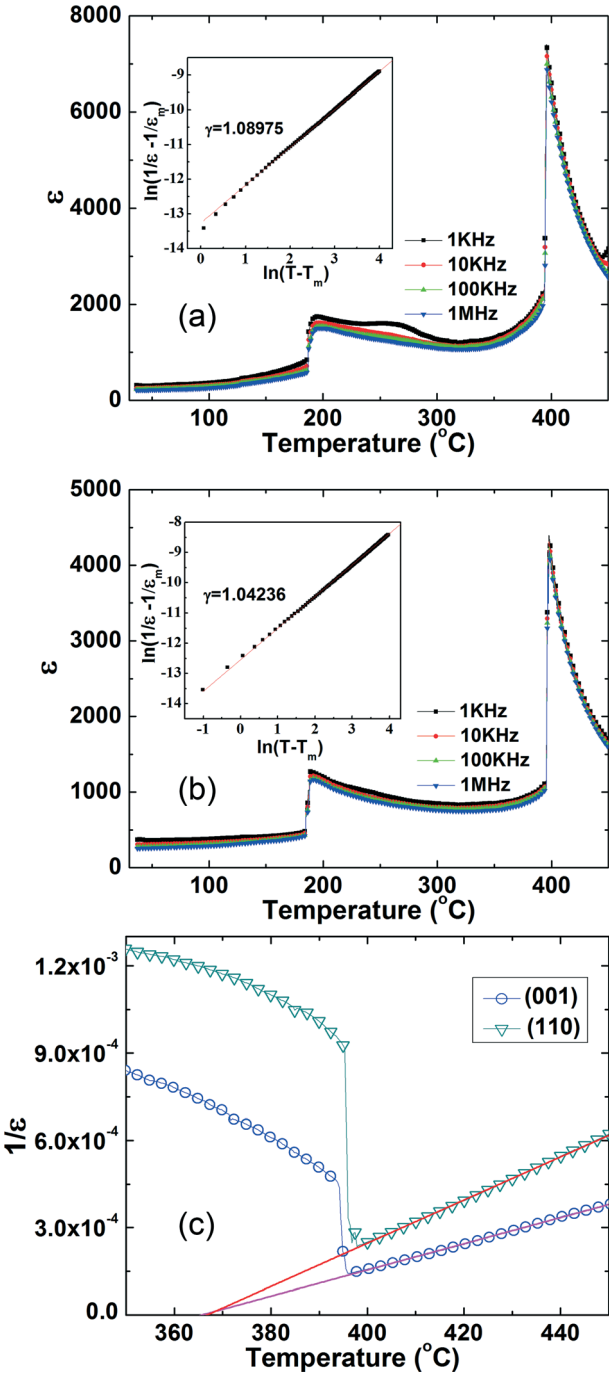

Fig. 3 (Color online) Temperature dependence of the dielectric constants of (a) $(100)_{pc}$ and (b) $(110)_{pc}$ oriented KNN25/75 crystals at different frequencies. The insets show their respective $\ln(1/\varepsilon - 1/\varepsilon_m)$ *vs.* $\ln(T - T_m)$ curves. (c) $1/\varepsilon$ *vs.* T curves of $(100)_{pc}$ and $(110)_{pc}$ oriented KNN25/75 crystals.

indicates an orthorhombic symmetry of the KNN crystals.[23,24] The peaks of the single crystal shifted to a higher angle compared with those of the starting polycrystalline powder, implying the volume decrease of the unit cell. Since the ionic radius of sodium is smaller than that of potassium, it is reasonable to consider that the decrease of the unit cell is induced by the decrease of potassium content in the single crystal caused by segregation. The XRF results show the ratio of K : Na : Nb to be 0.25 : 0.75 : 1.00 with a maximum error of ±2.5% and further support the aforementioned estimations. The effective segregation coefficients K_{eff}, ($K_{eff} = C_S/C_L(\infty)$), of K and Na ions are calculated to be 0.36 and 2.8, respectively. The 2θ–ω scans of the $(100)_{pc}$ and $(110)_{pc}$ oriented single crystals are shown in Fig. 2(b). The XRD rocking curves of the $(200)_{pc}$ and $(110)_{pc}$ diffraction peaks have full width at half maximum (FWHM) of 2.9 and 1.8 arcmin, respectively, implying relatively high quality of the as-grown crystals.

Investigation into the dielectric properties of the KNN single crystals along different orientations reveals anisotropic behavior. Fig. 3 illustrates the temperature dependence of the dielectric constant (ε) of the $(100)_{pc}$ and $(110)_{pc}$ oriented KNN25/75 crystals at different frequencies. The dielectric constants of both $(100)_{pc}$ and $(110)_{pc}$ plates show a sharp peak at ~396 °C, suggesting the ferro-to-paraelectric phase transition from the tetragonal ($P4mm$) to the cubic phase ($Pm3m$).[25] Moreover, another dielectric anomaly peak appears at ~187 °C, which can be attributed to the phase transition from the orthorhombic ($Amm2$) to the tetragonal ($P4mm$) phase.[26] The temperatures of every dielectric peak are consistent with each other at different orientations within experimental error. The detailed dielectric and piezoelectric properties of the single crystals are summarized in Table 1.

For the two directions, the dielectric constants slightly decreased with the increase of frequencies. It's not very obvious, nonetheless this phenomenon is evidence indicating some relaxation behavior. The dielectric dispersion behavior in KNN25/75 can be evaluated using a modified Curie–Weiss law,[27] $\frac{1}{\varepsilon} - \frac{1}{\varepsilon_m} = \frac{(T - T_m)^\gamma}{C_1}$, where γ is the diffusivity parameter, C_1 is the Curie-like constant and T_m is the temperature at which ε is maximum (ε_m). The value of γ approaches 1 in the case of a normal ferroelectric, whereas the value will be 2 for an ideal relaxor ferroelectric. The insets in Fig. 3 show the logarithm of $(1/\varepsilon - 1/\varepsilon_m)$ against the logarithm of $(T - T_m)$. The diffusivity parameter γ is calculated from the slope. By linear fitting, it's shown that the γ indexes for $(100)_{pc}$ and $(110)_{pc}$ orientations are 1.08975 and 1.04236, respectively, very close to 1, revealing that ε obeys the Curie–Weiss law,

Table 1 Dielectric, piezoelectric and ferroelectric properties of $(100)_{pc}$ and $(110)_{pc}$ orientated KNN25/75 single crystals (ε_{rt} represents the dielectric constant at room temperature)

Orientation	ε_{rt}	ε_m	P_r (μC cm^{-2})	E_c (kV mm^{-1})	d_{33} (pC N^{-1})	Strain (%)	k_t
$(100)_{pc}$	375	7407	7.2	0.84	145	0.025	0.69
$(110)_{pc}$	423	4395	10.2	0.61	70	0.05	0.51

$\varepsilon = \frac{C}{T - T_c}$. Here, C and T_C are the Curie–Weiss constant and the Curie–Weiss temperature, respectively. As seen in Fig. 3(c), the $1/\varepsilon$ *versus* T curves of the two orientations fit the law very well, indicating that the substitution of Na^+ for K^+ in the lattice sites didn't cause cation disorder. The Curie–Weiss temperature for $(100)_{pc}$ is 366 °C and for $(110)_{pc}$ 367 °C, and the discrepancy between the two values can be neglected within experimental error. The Curie–Weiss constants are 2.2×10^5 K for $(100)_{pc}$ and 1.3×10^5 K for $(110)_{pc}$, demonstrating the anisotropy of the cubic phase KNN.

The piezoelectric and ferroelectric properties of $(100)_{pc}$ and $(110)_{pc}$ orientated KNN25/75 crystals are shown in Table 1. The ferroelectric parameters were taken from room-temperature polarization and strain hysteresis loops in Fig. 4 and the electromechanical coupling coefficients (k_t) were calculated according to the impedance spectra in Fig. 5 using the following formula: $k_t^2 = \frac{\pi}{2}\frac{f_r}{f_a}\tan\left(\frac{\pi}{2}\frac{f_a - f_r}{f_a}\right)$, where f_r and f_a represent the resonant and antiresonant frequencies. The piezoelectric coefficient (d_{33}) of the $(100)_{pc}$ orientated crystal (~145 pC N^{-1}) is much higher than that of $K_{0.5}Na_{0.5}NbO_3$ single crystals prepared by solid-state crystal growth (80 pm V^{-1}).[12] The crystals also show a superior thickness electromechanical coupling property (k_t = 0.69). However, the electromechanical coupling (k_t) and piezoelectric coefficients (d_{33}) of the $(110)_{pc}$ oriented crystal were only 0.51 and 70 pC N^{-1}, respectively. This obvious anisotropy derives from other mechanisms rather than the inherent crystallographic anisotropy, which will be discussed in detail later.

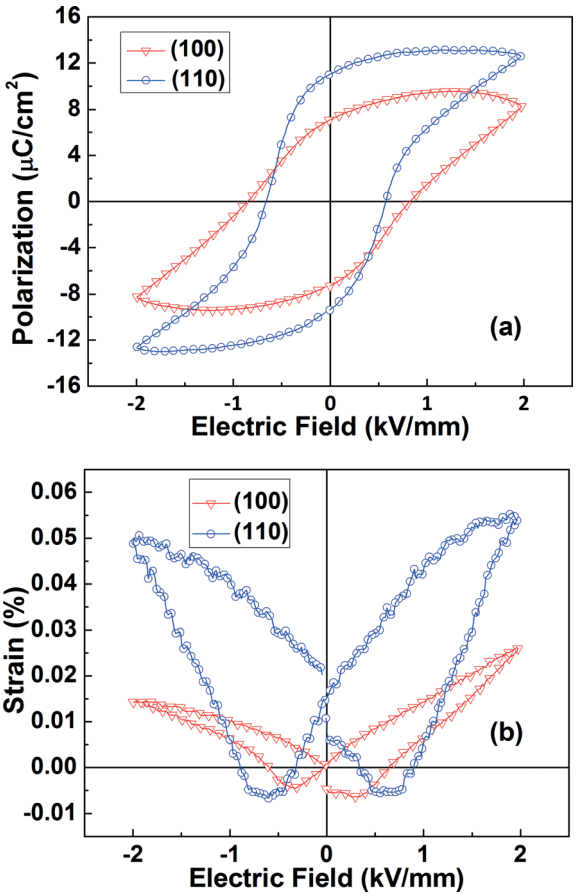

Fig. 4 (Color online) (a) Polarization and (b) strain hysteresis loops of $(100)_{pc}$ and $(110)_{pc}$ oriented KNN25/75 single crystals at room temperature.

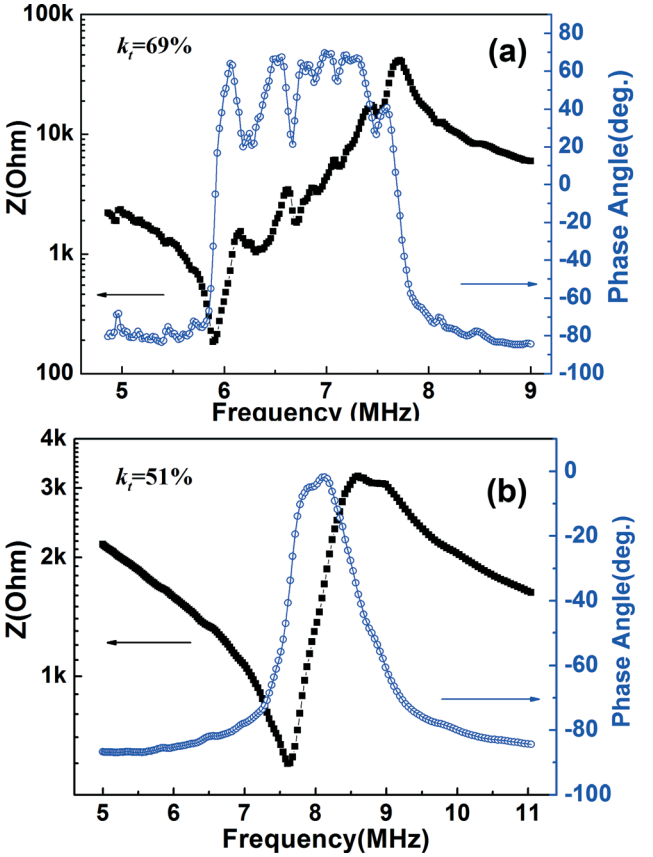

Fig. 5 (Color online) The impedance and phase angle spectra of (a) $(100)_{pc}$ and (b) $(110)_{pc}$ oriented KNN25/75 crystals at room temperature.

It can be seen in Fig. 4 that the remanent polarization (P_r) of the $(100)_{pc}$ oriented crystals (7.2 μC cm^{-2}) is smaller than that of $(110)_{pc}$ (10.2 μC cm^{-2}). The ratio of remanent polarization along $(100)_{pc}$ to $(110)_{pc}$ is 1 : 1.42, which is very close to $1 : \sqrt{2}$. On the other hand, the d_{33} value of the $(100)_{pc}$ samples is superior to that of $(110)_{pc}$ ones. Both these phenomena can be explained by the theory of the engineered domain configuration.[28] The schematics of domain configurations for unpoled and poled $(100)_{pc}$ orthorhombic crystals are illustrated in Fig. 6(a). For orthorhombic single crystals, the polar direction is along $<110>_{pc}$. Unpoled orthorhombic single crystals have the configuration wherein the polar vectors are randomly orientated along 12 equivalent $<110>_{pc}$ directions. When poled along $[100]_{pc}$, the crystal reached a domain engineering state in which each domain has one of four possible polar directions ($[110]_{pc}$, $[1\bar{1}0]_{pc}$, $[\bar{1}10]_{pc}$, $[\bar{1}\bar{1}0]_{pc}$). So the remanent polarization of $[100]_{pc}$ should be the projection of the polarization

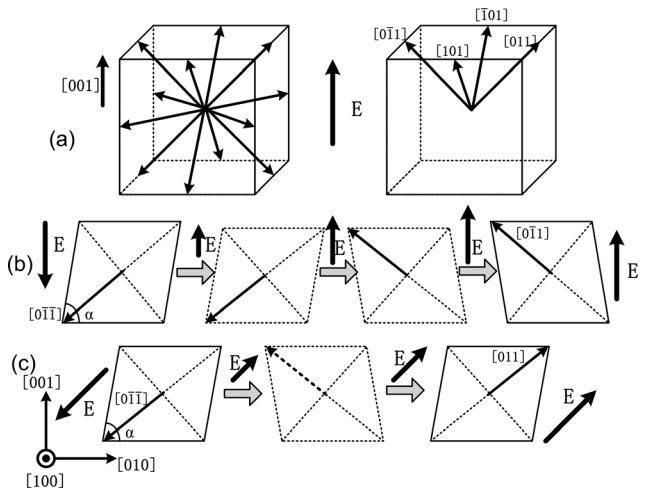

Fig. 6 (Color online) (a) Schematics of domain configurations for $(100)_{pc}$-oriented orthorhombic KNN25/75 crystals. The left panel: in the unpoled state, the polarization vectors are along twelve equivalent $(110)_{pc}$ directions. The right panel: poled along $(100)_{pc}$, only 4 polarization directions are left. (b) The domain switching process of one domain in $(100)_{pc}$ crystals and (c) in $(110)_{pc}$ crystals.

vector along $[110]_{pc}$. As for the $(110)_{pc}$ orientated crystal, a single domain state can be expected if the complete poling state is achieved. That's why the remnant polarization of $(100)_{pc}$ oriented KNN25/75 crystals should be $1/\sqrt{2}$ of that of the $(110)_{pc}$ oriented crystals'. However, the single domain configuration is not stable because of the high elastic and electrostatic energy. The $(110)_{pc}$ oriented crystal would depolarize when the electric field is removed, which results in inferior electromechanical coupling coefficients and piezoelectric properties.

The reason that the $(110)_{pc}$ orientation exhibited a larger strain than $(100)_{pc}$ could be understood from the schematic diagram of the hypothesis model illustrated in Fig. 6(b) and (c). Fig. 6(b) shows the switching process of one domain in $(001)_{pc}$ oriented crystals when an alternating electric field was applied along the $[001]_{pc}$ direction. Firstly, the domains orientated along $[\bar{1}\bar{1}0]_{pc}$ when a $[00\bar{1}]_{pc}$ direction electric field was applied. When a reversed electric field less than the coercive field was applied to the polarized $<100>_{pc}$ KNN, the lattice of KNN contracted along the direction of the electric field. With further increase in the reversed electric field, ferroelectric domains underwent a 90° reorientation. Obviously, domain switching contributes little to the strain along $[100]_{pc}$. Once the reversed electric field exceeds the coercive field, the strain is mainly caused by lattice elongation induced by the converse piezoelectric effect. On the contrary, the strain along $[110]_{pc}$ was mainly induced by the two-step 90° domain-switching process.[29] Firstly, the polarization vector switched 90° and induced contraction of the lattice parameters along the $[110]_{pc}$ direction. Subsequently, another 90° polarization reorientation took place and the corresponding lattice parameters were elongated. So we assumed that the distinction between strains along $(100)_{pc}$ and $(110)_{pc}$ originated from the difference of mechanisms that make dominant contributions to the strains, *i.e.* a domain-switching process or a converse piezoelectric effect.

The comparison of the electric properties and dimensions of KNN-based crystals grown by different methods is given in Table 2. It can be seen that our single crystal is the largest achieved up to now and its thickness electromechanical coupling factors, k_t, are on a relatively high level. Besides, the single crystal diffraction data further confirm that the as-grown transparent single crystal is of high quality. However, the *P–E* loop is not totally saturated, which might be attributed to the leakage current induced by oxide vacancies.[19] Some modifications such as Mn-doping[17] or annealing process would be carried out in future studies to further improve the quality of KNN single crystals.

Conclusions

In summary, high quality $(K_{0.25}Na_{0.75})NbO_3$ single crystals with dimensions of up to Ø30mm × 10 mm were grown by a carefully controlled TSSG method. XRD patterns indicate that the KNN25/75 single crystal has an orthorhombic perovskite-type structure at room-temperature. The room-temperature dielectric constants for the $(100)_{pc}$ and $(110)_{pc}$ oriented crystal samples are found to be 375 and 423 at 1 kHz, respectively. The piezoelectric constant d_{33} and the thickness electromechanical coupling factor k_t are 145 pC N^{-1} and 69% for the $(100)_{pc}$ oriented crystal and 70 pC N^{-1} and 51% for the $(110)_{pc}$ oriented crystal, revealing a domain engineering effect. Furthermore, a larger strain was achieved along $(110)_{pc}$ than along the $(100)_{pc}$ orientation. This anisotropic behavior is explained by domain switching.

Table 2 Comparison of some properties of KNN crystals grown by different methods

	ε_{rt}	k_t	d_{33} (pC N^{-1})	T_c (°C)	Method	Dimensions	Ref.
KNN25/75	375	0.69	145	396	TSSG	Ø30 × 10 mm^3	This work
$K_{0.47}Na_{0.53}NbO_3$	600	—	110	390	Flux	2 × 2 × 2 mm^3	17
KNN (B_2O_3 Flux)	~1000	—	106	413	Flux	4 × 6 × ~ mm^3	18
$K_{0.5}Na_{0.5}NbO_3$	1015	—	80	410	Solid state	4 mm	12
0.95KNN–0.05$LiNbO_3$	185	0.61	405	426	Bridgman	4 × 6 × 0.5 mm^3	19
(Na,K)(Nb,Ta)O_3	267	0.646	162–200	298	TSSG	12 × 12 × 11 mm^3	21
$Li_{0.02}(Na_{0.5}K_{0.5})_{0.98}NbO_3$	164	0.7	—	—	TSSG	—	20

Acknowledgements

This work was financially supported by the Ministry of Science and Technology of China through the 973 Program (no. 2013CB632902-3, 2013CB6329052 and 2013CB632906), the Natural Science Foundation of China (no. 51332009, 51372258, 11304333, 61001041, 11090332 and 51272268), the Science and Technology Commission of Shanghai Municipality (no. 12DZ0501000), the Fund of Shanghai Institute of Ceramics (no. Y29ZC4140G and Y39ZC4140G), and Shanghai Municipal Electric Power Company (no. 52091413502 W).

References

1 Q. M. Zhang, H. Wang, N. Kim and L. E. Cross, *J. Appl. Phys.*, 1994, **75**, 454–459.
2 C. He, X. Z. Li, Z. J. Wang, Y. Liu, D. Q. Shen, T. Li and X. F. Long, *CrystEngComm*, 2012, **14**, 4513–4519.
3 Y. Liu, X. Z. Li, Z. J. Wang, C. He, T. Li, L. D. Ai, T. Chu, D. F. Pang and X. F. Long, *CrystEngComm*, 2013, **15**, 1643–1650.
4 Y. Saito, H. Takao, T. Tani, T. Nonoyama, K. Takatori, T. Homma, T. Nagaya and M. Nakamura, *Nature*, 2004, **432**, 84–87.
5 W. W. Ge, J. F. Li, D. Viehland, Y. F. Chang and G. L. Messing, *Phys. Rev. B: Condens. Matter Mater. Phys.*, 2011, 83.
6 Y. P. Guo, K. Kakimoto and H. Ohsato, *Appl. Phys. Lett.*, 2004, **85**, 4121–4123.
7 R. Z. Zuo, X. S. Fang and C. Ye, *Appl. Phys. Lett.*, 2007, **90**, 092904.
8 P. Zhao, B. P. Zhang and J. F. Li, *Appl. Phys. Lett.*, 2007, **91**, 172901.
9 D. Lin, K. W. Kwok and H. L. W. Chan, *J. Appl. Phys.*, 2007, **102**, 034102.
10 J. G. Fisher, A. Bencan, J. Holc, M. Kosec, S. Vernay and D. Rytz, *J. Cryst. Growth*, 2007, **303**, 487–492.
11 J. G. Fisher, A. Bencan, M. Kosec, S. Vernay and D. Rytz, *J. Am. Ceram. Soc.*, 2008, **91**, 1503–1507.
12 H. Ursic, A. Bencan, M. Skarabot, M. Godec and M. Kosec, *J. Appl. Phys.*, 2010, **107**, 033705.
13 G. Shirane, R. Newnham and R. Pepinsky, *Phys. Rev.*, 1954, **96**, 581–588.
14 M. Ahtee and A. M. Glazer, *Acta Crystallogr., Sect. A: Cryst. Phys., Diffr., Theor. Gen. Crystallogr.*, 1976, **32**, 434–446.
15 I. P. Raevskii, M. P. Ivliev, L. A. Reznichenko, M. N. Palatnikov, L. E. Balyunis and M. A. Malitskaya, *Tech. Phys.*, 2002, **47**, 772–776.
16 D. B. Lin, Z. R. Li, Z. Xu and X. Yao, *Ferroelectrics*, 2009, **381**, 1–8.
17 Y. Kizaki, Y. Noguchi and M. Miyayama, *Key Eng. Mater.*, 2007, **350**, 85–88.
18 R. Saravanan, D. Rajesh, S. V. Rajasekaran, R. Perumal, M. Chitra and R. Jayavel, *Cryst. Res. Technol.*, 2013, **48**, 22–28.
19 K. Chen, G. S. Xu, D. F. Yang, X. F. Wang and J. B. Li, *J. Appl. Phys.*, 2007, **101**, 044103.
20 M. Davis, N. Klein, D. Damjanovic, N. Setter, A. Gross, V. Wesemann, S. Vernay and D. Rytz, *Appl. Phys. Lett.*, 2007, **90**, 062904.
21 L. M. Zheng, X. Q. Huo, R. Wang, J. J. Wang, W. H. Jiang and W. W. Cao, *CrystEngComm*, 2013, **15**, 7718–7722.
22 B. Jaffe, W. R. Cook and H. L. Jaffe, *Piezoelectric ceramics*, Academic Press, London, New York, 1971.
23 J. Attia, L. Bellaiche, P. Gemeiner, B. Dkhil and B. Malic, *J. Phys. IV*, 2005, **128**, 55–60.
24 D. B. Lin, Z. R. Li, S. J. Zhang, Z. Xu and X. Yao, *J. Am. Ceram. Soc.*, 2010, **93**, 941–944.
25 D. W. Baker, P. A. Thomas, N. Zhang and A. M. Glazer, *Acta Crystallogr., Sect. B: Struct. Sci.*, 2009, **65**, 22–28.
26 J. A. Baier-Saip, E. Ramos-Moor and A. L. Cabrera, *Solid State Commun.*, 2005, **135**, 367–372.
27 K. Uchino and S. Nomura, *Ferroelectrics*, 1982, **44**, 55–61.
28 S.-E. Park and T. R. Shrout, *J. Appl. Phys.*, 1997, **82**, 1804.
29 B. Jiang, Y. Bai, W. Y. Chu, Y. J. Su and L. J. Qiao, *Appl. Phys. Lett.*, 2008, **93**, 152905.

